Advanced MRI in inflammatory arthritis

van der Leij, C.

Chapter 3

Reproducibility of DCE-MRI time–intensity curve-shape analysis in patients with knee arthritis: A comparison with qualitative and pharmacokinetic analyses

Christiaan van der Leij, Cristina Lavini, Marleen G.H. van de Sande,
Marjolein J.H. de Hair, Christophe Wijffels, Mario Maas

J. Magn. Reson. Imaging 2015;42:1497–1506.

Abstract

Purpose
To compare the between-session reproducibility of dynamic contrast-enhanced magnetic resonance imaging (DCE-MRI) combined with time-intensity curve (TIC)-shape analysis in arthritis patients, within one scanner and between two different scanners, and to compare this method with qualitative analysis and pharmacokinetic modeling (PKM).

Materials and methods
Fifteen knee joint arthritis patients were included and scanned twice on a closed-bore 1.5T scanner (n=9, group 1), or on a closed-bore 1.5T and on an open-bore 1.0T scanner (n=6, group 2). DCE-MRI data were post-processed using in-house developed software ("Dynamo"). Disease activity was assessed.

Results
Disease activity was comparable between the two visits. In group 1 qualitative analysis showed the highest reproducibility with intraclass correlation coefficients (ICCs) between 0.78 and 0.98 and root mean square-coefficients of variation (RMS-CoV) of 8.0%–14.9%. TIC-shape analysis showed a slightly lower reproducibility with similar ICCs (0.78–0.97) but higher RMS-CoV (18.3%-42.9%). The PKM analysis showed the lowest reproducibility with ICCs between 0.39 and 0.64 (RMS-CoV 21.5%–51.9%). In group 2 TIC-shape analysis of the two most important TIC-shape types showed the highest reproducibility with ICCs of 0.78 and 0.71 (RMS-CoV 29.8% and 59.4%) and outperformed the reproducibility of the most important qualitative parameter (ICC 0.31, RMS-CoV 45.1%) and the within-scanner reproducibility of PKM analysis.

Conclusion
TIC-shape analysis is a robust post-processing method within one scanner, almost as reproducible as the qualitative analysis. Between scanners, the reproducibility of the most important TIC-shapes outperform that of the most important qualitative parameter and the within-scanner reproducibility of PKM analysis.

Introduction

Dynamic contrast-enhanced magnetic resonance imaging (DCE-MRI) is a commonly used method which involves the sampling of MRI signal intensity in time, during the intravenous injection of a contrast agent. The acquired, consecutive MRI samples result in time–intensity curves (TIC), which can be analyzed to extract relevant parameters.

Three post-processing methods are generally utilized, with the qualitative analysis being the most common and straightforward approach. With this method parameters such as the initial rate of enhancement or early enhancement rate (IRE/EER) or the maximal enhancement (ME) can be obtained directly from the TICs. This approach has the advantage of being fast and readily available on many software packages, but the values of the produced parameters depend significantly on the magnet field strength and on the sequence parameters used.

Another approach is to calculate absolute physiology related parameters such as the volume transfer coefficient, K^{trans}, the volume of the extracellular extravascular space, V_e, and the rate constant, K_{ep} ($K_{ep}=K^{trans}/V_e$), by using pharmacokinetic models (PKM) eg, by Tofts et al.[1] This method is assumed to provide outcomes that are independent of system hardware and field strength, but it is technically and computationally demanding. Moreover, parameter outcomes are dependent on the model used and it requires additional sequences to compute the absolute contrast agent concentration, which makes it impractical in clinical (non research) settings.

A third, more recently introduced method classifies differently shaped TICs pixel-by pixel into seven TIC-shape categories, and proposes the calculation of absolute and relative number of these TIC-shape categories within a volume of interest as a disease-related parameter.[2] This method is thought to be more robust compared to the qualitative analysis, is much less computationally demanding compared to PK modeling, is model-independent, and does not require the knowledge of the absolute contrast agent concentrations.

DCE-MRI combined with any of these three post-processing methods is used to study synovial inflammation, either as discriminator in (early) arthritis patients[3–9] or to assess the response to various treatments.[7,8,10–19] However, data on the reproducibility of these methods in these patient groups is scarce and mainly focused on the intra- and interobserver variation.

As TIC-shape analysis is relatively easy, fast, and costeffective, we believe that this post-processing technique is ideal to study synovial inflammation, but reliability still has to be shown. The goal of this study, therefore, was to compare the between-session reproducibility of DCE-MRI combined with TIC shape analysis in arthritis patients, within one scanner and between two different scanners with different field strengths, and to compare this method with the two other post-processing methods.

Materials and methods

Patients

Group 1: Within scanner reproducibility

Ten consecutive patients from an early arthritis cohort[20] (onset of disease <1 year) were included between February and August 2008. All the patients included had affected knee joints. Exclusion criteria were current or previous use of disease-modifying anti rheumatic drugs (DMARDs) and/or glucocorticoids for joint complaints, an elevated serum creatinine, claustrophobia, or other contraindications for MRI investigation. One patient was excluded due to technical problems that occurred during one of the examinations. A total of nine patients were included in this group, five male and four female. Median age was 51 years (range, 28–82). The diagnostic classifications were: rheumatoid arthritis (RA) (according to the 1987 American College of Rheumatology classification criteria for RA[21]) in two patients, osteoarthritis[22] in two patients, Lyme associated arthritis in one patient, spondyloarthritis[23] in one patient, and undifferentiated arthritis in three patients. Seven right knees and two left knees were scanned.

Group 2: Between scanner reproducibility

RA patients with longstanding stable disease activity were included for the between-scanner reproducibility between June and July 2009. A knee joint had to be affected. Exclusion criteria for this group were the same as for group 1, except for the use of medication. The goal was to include 10 RA patients, but due to the fact that one of the MRI scanners was replaced, inclusion halted at six patients, one male and five female. Median age was 51.5 year (range 26–65). Patients were classified as: RA in four patients, juvenile idiopathic arthritis[24] in one patient, and remitting seronegative symmetrical synovitis with pitting edema[25] in one patient. Five left knees and one right knee were scanned.
The study was approved by the local Institutional Review Board and patients gave written informed consent.

Study design

Patients in both groups 1 and 2 underwent a DCE-MRI of the affected knee joint at two timepoints with 1 week in between. Patients were scanned on the same day of the week at the same time of day to minimize the effect of daily exercise. When this was not possible, the second scan was made within 1 week, but at the same time of day.

Disease activity

At both timepoints a trained rheumatology investigator with 4 years of experience in rheumatology research (M.v.d.S.) assessed the disease activity. The disease activity parameters used were the 28-tender and swollen joint count (28TJC/28SJC) score, the visual analog scale (VAS) of disease activity and of pain (both indicated by the patient), the duration of morning stiffness in minutes, and the local pain and swelling score (assessed by the investigator).

Within-scanner reproducibility: Group 1

The MRI studies were performed on a 1.5T system (GE Signa Horizon Echospeed, LX9.0, General Electric Medical Systems, Milwaukee, WI) using a dedicated knee coil (quadrature detection).
At each session the diagnostic images required for disease assessment were obtained first. Care was taken when manually repositioning the patient in the same position on both examinations. The positioning was done on anatomical landmarks.
Both times, a dynamic series of 20 consecutive images of 20 slices were acquired using the following imaging parameters: TR/TE/flip angle58.1/3.5msec/30, slice thickness 4 mm, field of view (FOV) 18 cm, 256*256 matrix, axial orientation. The duration of each dynamic scan was 21.95 seconds. The total imaging time of the dynamic series was 7 minutes 19 seconds. A bolus of 0.1 mmol/kg contrast agent (Magnevist, Schering, Berlin, Germany) was administered after 60 seconds at a rate of 5 ml/second, followed by a 15-ml saline bolus using an automated injector (MEDRAD, Spectris). Care was taken to administer exactly the same amount of contrast agent in the same antecubital vein, using an infusion needle of the same size both times.

Between-scanner reproducibility: Group 2

The six patients included in this group were scanned once on the 1.5T scanner using the parameters described above, and once on an open-bore 1T scanner (Panorama Philips, Best, the Netherlands) using the following parameters: TR/TE/flip angle 10.4/6.9msec/30 slice thickness 4 mm, FOV 18 cm, 256*256 matrix, axial orientation. These parameters were chosen to match the spatial and temporal resolution of the 1.5T scan as closely as possible. The total imaging time of the dynamic contrast enhanced acquisition was 7 minutes 22 seconds. All other parameters (eg, patient placement, contrast dose, and infusion rate) were identical to the scans of group 1.

Data

Qualitative and TIC-shape analysis

Images obtained with the DCE-MRI acquisition were transferred to a standard PC workstation for analysis. This was performed using an in-house written analysis package

(called "Dynamo"[26] running on MatLab, MathWorks, Natick, MA). This was done by an investigator with more than 6 years experience with the analysis program (C.v.d.L.). This software does not allow for total blinding of patient characteristics; therefore, the images acquired at both timepoints were randomly analyzed in batches in separate sessions weeks apart. Parametric maps of all images were created showing the seven defined TIC types: TIC-shape type 1: no enhancement, type 2: gradual enhancement, types 3–5: early enhancement followed by plateau phase (3), early washout (4), persistent enhancement (5), type 6: artery, type 7: other (Figure 3.1),2 as well as maps showing the ME, slope of early enhancement (Slope), and time to peak (TTP). The analyzed volume consisted of 12 axial images, comprising almost 5 cm of the joint in the long axis of the knee. As the most distal border, we selected the image that showed the tibial plateau. Care was taken to select the best matching image from both acquisitions.

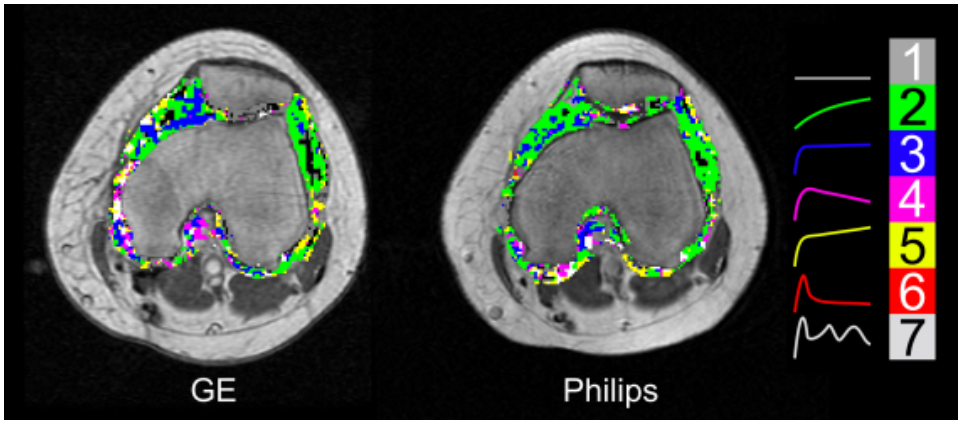

Figure 3.1 Comparison of slices from the same patient in two consecutive scans on the same scanner (GE Signa Horizon Echospeed, 1.5T) with TIC-shape type maps superimposed. TIC-shape types: 1: no enhancement, 2: gradual enhancement, 3–5: early enhancement followed by plateau phase (3), early washout (4), persistent enhancement (5), 6: artery, 7: other.

Regions of interest (ROIs) were drawn around the synovium (Figure 3.1) on the 12 selected slices, excluding enhancing muscle tissue and skin, creating therefore a 3D ROI volume. This was done on the ME maps, because of the increased conspicuity of synovial tissue on these maps. Postcontrast T1-weighted images from the dynamic series were used to check the accurateness of the ROIs.

The absolute and relative number of TIC-shapes (ie, the absolute number of a specific TIC-shape divided by the number of all enhancing TIC-shapes together in a 3D ROI) per patient was used for statistical analysis. As qualitative parameters we used the ROI-averaged value (referred to as the "mean") of the ME, TTP, and the Slope. We also tested the enhancing volume (ie, the volume of a single pixel times the number of all

enhancing pixels, EV) between the two examinations. A pixel was considered to be enhanced when its ME value was higher than 30%.

Pharmacokinetic modeling analysis

On the data of group 1 we performed quantitative analysis by applying Tofts' model. Data were analyzed using the same software package ("Dynamo"). First the absolute precontrast T1 relaxation maps were calculated by fitting the data obtained with a variable flip angle fast spoiled gradient echo (FSPGR) sequence. The signal intensities were transformed into signal concentrations (in each voxel) using the precontrast T1 maps with the relationship[27]:

$$C_{Gd}(t) = -\frac{1}{TR \cdot \Re_1}\left\{\ln\left(\frac{SE(t)\cdot\left(e^{-\frac{TR}{T_{10}}}-1\right)+e^{-\frac{TR}{T_{10}}}\left(1-\cos\vartheta\right)}{1+\cos\vartheta\left(SE(t)\left(e^{-\frac{TR}{T_{10}}}-1\right)-1\right)}\right)-\frac{TR}{T_{10}}\right\} \quad \text{Eq. (1)}$$

where *SE(t)* represents the signal enhancement at time t *(SE(t)=(S(t)-S(0))/S(0))*, and S(0) is the signal intensity before contrast injection, $\Re_1$ represents the tissue relaxivity (we used the value $\Re_1$ 154.52 s-1 mM-1 lt), θ ; is the flip angle, and T_{10} the native T1 as calculated with the variable flip angle method. We applied Tofts' model in its extended form[1]:

$$C_t(t) = v_p C_p(t) + K_{trans} \cdot C_p(t) \otimes e^{-\frac{K^{trans}}{v_e}t} \quad \text{Eq. (2)}$$

where C(t) is the tissue concentration at time t as calculated with Eq. (1) and $C_p(t)$ is the arterial input function (AIF), ie, the plasma concentration of contrast agent in the capillaries feeding the tissue. K^{trans} is the volume transfer constant from the plasma to the extracellular space v_e, v_p is the plasma space. The reverse transfer constant k_{ep} is defined as $k_{ep}=K^{trans} / v_e$.[1]

In order to measure the AIF we manually selected an ROI in the popliteal artery in multiple sections of the scan. An arterial concentration–time curve $C_{blood}(t)$ was obtained using Eq. (1), and by using $T_{10Blood}$=1540 msec. Plasma concentration in the capillary was estimated using:

$C_{plasma}= C_{blood}/(1-Hct)$.[28]

with Hct=hematocrit, Hct=0.45.

To avoid partial volume effects, only the pixels with the highest enhancement were used.[28]
The resulting plasma concentration time curve was fitted to:

$$C_p(t) = \beta\left(\chi \cdot t \cdot e^{-mb \cdot t} - e^{-mb \cdot t} + e^{-ma \cdot t}\right) \quad \text{Eq. (3)}$$

in order to provide $C_p(t)$, a functional form that would allow Eq. (2) to be solved in closed form:

$$C_{tiss}(t) = \beta\left\{v_i\left(\chi \cdot t \cdot e^{-mbt} - e^{-mbt} + e^{-mat}\right) + v_e k_{ep}\left[\frac{\chi}{k_{ep} - mb}\left(t \cdot e^{-mbt} - \frac{\left(e^{-mbt} - e^{-k_{ep} \cdot t}\right)}{k_{ep} - mb}\right) + \frac{(e^{-mat} - e^{-k_{ep} \cdot t})}{k_{ep} - ma} - \frac{\left(e^{-mbt} - e^{-k_{ep} \cdot t}\right)}{k_{ep} - mb}\right]\right\} \quad \text{Eq. (4)}$$

Eqs. (3) and (4) are formally identical to Eqs. (3) and (7) in.[29]
The PKM parameters K^{trans}, v_e, v_i, and $k_{ep}=K^{trans}*v_e$ were calculated by fitting Eq. (4) to the calculated concentration–time curves in the tissue and using the patient specific AIF as described above. Nonlinear fitting was done on a voxel-by-voxel basis, using the Levenberg-Marquardt fitting algorithm.
Pharmacokinetic modeling analysis was not performed on the six patients in group 2, as there was no possibility to perform a reliable pre-DCE-MRI scan T1-mapping sequence at the time of acquisition on the 1.0T system.

Statistical analysis

Statistical software (SPSS v. 20, IBM, Armonk, NY) was used for the analysis.
The reproducibility between scan 1 and scan 2 was analyzed using the intraclass correlation coefficient (ICC) and the root mean square coefficient of variation (RMS-CoV) as described by Roberts et al.[30] For ICC, a 2-way random model was used with absolute agreement, single measures, and a confidence interval of 95%. ICC scores were classified as "poor" when below 0.20, as "fair" when between 0.20 and 0.40, as "moderate" when between 0.40 and 0.60, as "good" when between 0.60 and 0.80, and as "very good" when above 0.80. *P*-value for statistical significance was set at <.05. The disease activity parameters were tested for significant differences between two scan moments using the nonparametric Wilcoxon signed rank test.

Results

Within scanner reproducibility: Group 1

Disease activity

All except one disease activity parameter were comparable between the two visits: a significantly higher VAS disease activity was observed at the second visit (Table 3.1). This parameter did not show a significant correlation with the observed MRI parameters (*P*-value range qualitative analysis: 0.14–1.00, TIC-shape analysis: 0.57-0.98, PKM: 0.38–0.83).

Table 3.1 Disease activity parameters Group 1 (within scanner reproducibility).

Parameter	Visit1	Visit2	*P*-value
TJC28 (0-28)	1 (0-14)	2 (0-15)	0.206
SJC28 (0-28)	2 (1-12)	1 (0-14)	0.854
VAS general disease activity (0-100)	43 (0-72)	50 (0-82)	0.018
VAS pain (0-100)	49 (0-70)	70 (0-80)	0.063
Morning stiffness (minutes)	15 (0-120)	20 (0-120)	0.713
Local knee pain (0-4)	0 (0-1)	1 (0-1)	0.083
Local knee swelling (0-4)	1 (1-1)	1 (0-1)	0.317

Values in medians (Range). TJC28: Tender Joint Count of 28 joints, SWC 28: Swollen Joint Count of 28 joints, VAS: visual analog scale.

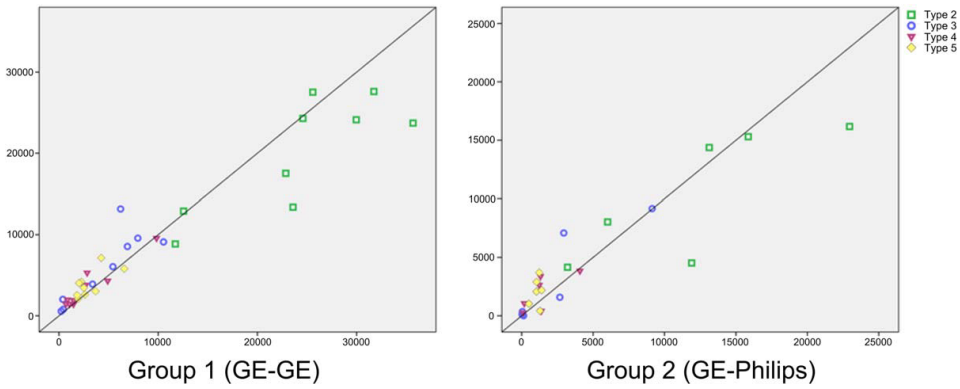

Figure 3.3 Total number of TIC-shapes per type in Group 1 (2 x GE, left) and Group 2 (y-axis GE, x-axis Philips; right). Lines: unity (y=x). Type2: green boxes, Type 3: blue circles, Type 4: pink triangles, type 5: yellow diamonds.

Qualitative parameters and volume

The mean value of the parameters ME, Slope, and TTP showed good to very good reproducibility, with ICCs ranging from 0.78 to 0.98 and RMS-CoV values ranging from

5.3% to 14.9% (Table 3.2). The EV showed a very good reproducibility with an ICC of 0.97 and an RMS-CoV of 8.7%.

TIC-shape absolute and relative amounts

The total number of enhancing pixels per TIC-shape type within the ROI showed good to very good reproducibility, with ICC values in the range of 0.78 to 0.97. RMS-CoV values ranged from 18.3% to 42.9%. The relative number of enhancing pixels per TIC-shape type showed lower reproducibility with ICC values in the range of 0.43 to 0.88 (moderate to very good). Observed RMS-CoV values, however, were in the same range as the values observed with total number of TIC shapes per type (19.5% to 44.8%) (Table 3.2).

Table 3.2 Qualitative and TIC-shape parameters Group 1 (within scanner reproducibility).

Parameter	Scan 1	Scan 2	ICC (95% CI)	RMS-CoV (%)
ME	1.26 (0.80-1.52)	1.27 (.82-1.60)	0.98 (0.89-0.99)	8,0
Slope	14.5 (12.7-19.7)	16.2 (13.5-24.9)	0.85 (0.20-0.97)	14.9
TTP (s)	209 (202-220)	202 (187-206)	0.78 (0.13-0.95)	5.3
EV (ml)	73.7 (46.8-87.8)	72.8 (51.9-90.0)	0.97 (0.88-0.99)	8.7
Tot type 2	24587 (17711-308587)	23716 (13148-25910)	0.83 (0.10-0.96)	18.3
Tot type 3	5431 (411-7422)	6056 (1408-9340)	0.90 (0.54-0.97)	42.9
Tot type 4	1474 (1474-3868)	1971 (1447-4804)	0.97 (0.82-0.99)	30.8
Tot type 5	2501 (2501-3968)	3459 (2576-4987)	0.78 (0.12-0.95)	27.0
Rel type 2 (%)	50.0 (41.0-61.0)	39.7 (32.1-50.4)	0.71 (-0.23-0.94)	19.5
Rel type 3 (%)	9.6 (1.4-13.9)	9.9 (3.5-20.8)	0.88 (0.37-0.98)	44.8
Rel type 4 (%)	4.4 (2.3-7.4)	5.4 (3.5-10.5)	0.88 (0.38-0.97)	31.5
Rel type 5 (%)	5.2 (4.4-8.3)	7.8 (6.4-9.0)	0.43 (-0.58-0.85)	27.2

Medians (Inter Quartile Range (IQR)). ICC: Intraclass Correlation Coefficient. RMS-CoV: Root Mean Square – Coefficient of Variation. ME: (Mean) Maximum Enhancement, Slope: Maximum observed enhancement slope between two time points, TTP: Time To Peak, EV: Volume of all enhancing pixels within the region of interest (ROI) Tot: total number of pixels within the Region of Interest (ROI) classified to the specific Time Intensity Curve (TIC) shape type. Rel: number of pixels within the ROI classified to the specific TIC shape type relative to all enhancing pixels within the ROI

Pharmacokinetic modeling analysis

For the PKM calculation, one patient was excluded due to false values on the created T_1-map of one of the scans. Therefore, the results from the PKM analysis are based on the eight remaining patients.

The parameter K^{trans} showed fair reproducibility, with an ICC of 0.39, and an RMS-CoV value of 51.9%. K_{ep} and V_e showed good reproducibility, with ICC values of respectively 0.62 and 0.64 and RMS-CoV values of 17.5% and 21.5% (Table 3.3).

Table 3.3 Pharmacokinetic Modelling parameters Group 1 (within scanner reproducibility).

Parameter	Scan 1 *	Scan 2 *	ICC (95%CI)	RMS-CoV (%)
K^{trans}	0.032 (0.030-0.059)	0.039 (0.023-0.092)	0.39 (-0.46-0.85)	51.9
k_{ep}	0.171 (0.122-0.215)	0.145 (0.131-0.239)	0.62 (-0.11-0.91)	17.5
v_e	0.424 (0.329-0.546)	0.387 (0.305-0.662)	0.64 (-0.11-0.92)	21.5

Values are shown as Medians (interquartile range, IQR). ICC: Intraclass Correlation Coefficient. RMS-CoV: Root Mean Square – Coefficient of Variation. K^{trans}: volume transfer coefficient, V_e: the volume of the extracellular extravascular space, K_{ep}: rate constant (K^{trans}/V_e)

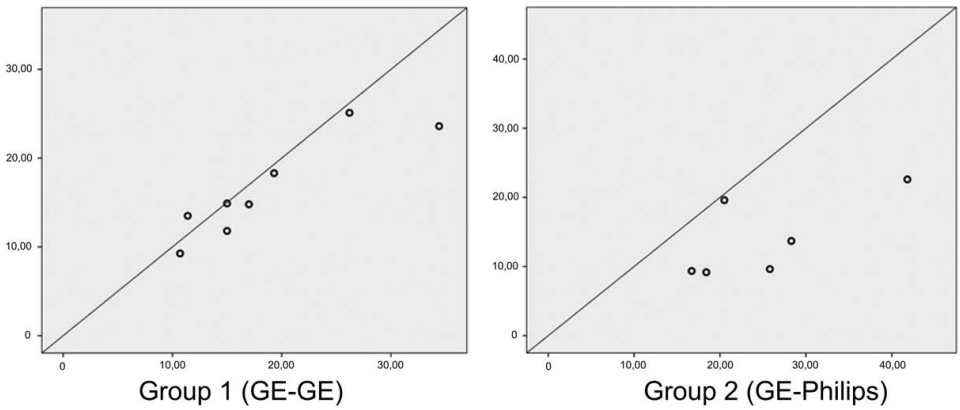

Figure 3.4 Measurement of Slope (in arbitrary units) in Group 1 (2 x GE, left) and Group 2 (y-axis GE, x-axis Philips; right). Lines: unity (y=x).

Inter-MRI variability: Group 2

Disease activity

No significant difference in disease activity was observed between either examination (Table 3.4).

Table 3.4 Disease activity parameters Group 2 (between scanner reproducibility).

Parameter	Visit1	Visit2	*P*-value
TJC28 (0-28)	1 (0-24)	0.5 (0-27)	0.414
SJC28 (0-28)	1 (0-21)	0 (0-22)	0.257
VAS general disease activity (0-100)	26 (0-88)	21.5 (3-78)	0.115
VAS pain (0-100)	25 (0-77)	14 (03-76)	0.673
Morning stiffness (minutes)	8.5 (0-120)	10.5 (0-150)	0.109
Local knee pain (0-4)	0 (0-1)	0.5 (0-1)	0.317
Local knee swelling (0-4)	0 (0-1)	0 (0-1)	1.000

Values in medians (Range). TJC28: Tender Joint Count of 28 joints, SWC 28: Swollen Joint Count of 28 joints, VAS: visual analog scale.

Qualitative parameters and volume

The statistical analysis showed lower ICC values for ME and Slope compared to the within-scanner reproducibility values. The ICC for the slope was fair (0.31) and for the ME good (0.63). The parameter TTP showed a moderate ICC value of 0.59. The RMS-CoV for these parameters ranged from 10.6% to 45.1%. The volume showed a very good reproducibility ICC value of 0.87 with an RMS-CoV of 33.6% (Table 3.5).

Table 3.5 Qualitative and TIC-shape parameters Group 2 (between scanner reproducibility).

Parameter	Scan 1	Scan 2	ICC (95% CI)	RMS-CoV (%)
ME	0.634 (0.331-1.215)	0.717 (0.323-0.884)	0.63 (-0.25-0.94)	25.7
Slope	11.7 (9.3-20.4)	23.2 (18.0-31.7)	0.31 (-0.12-0.82)	45.1
TTP (s)	153 (129-173)	191 (167-207)	0.59 (-0.11-0.93)	10.6
VE(ml)	39.4 (11.4-58.3)	36.9 (13.5-56.3)	.87 (0.31-0.98)	33.6
Tot type 2	11204 (4430-15522)	12516 (5317-17636)	0.78 (0.15-0.97)	29.8
Tot type 3	969 (97-7613)	1402 (44-4495)	0.89 (0.47-0.98)	73.8
Tot type 4	1844 (366-3491)	1273 (160-2048)	0.71 (0.02-0.95)	59.4
Tot type 5	2134 (882-3097)	1138 (903-1314)	0.09 (-0.34-0.73)	49.1
Rel type 2 (%)	27.1 (17.8-37.8)	42.0 (18.9-54.2)	0.54 (-0.14-0.91)	30.1
Rel type 3 (%)	2.5 (0.4-18.3)	4.1 (0.2-13.0)	0.92 (0.52-0.99)	79.8
Rel type 4 (%)	4.3 (1.5-9.1)	3.6 (0.5-7.5)	0.65 (-0.30-0.95)	66.3
Rel type 5 (%)	5.1 (3.6-7.4)	3.4 (3.0-4.2)	-0.30 (-0.78-0.56)	58.0

Medians (interquartile range, IQR). ICC: Intraclass Correlation Coefficient. RMS-CoV: Root Mean Square – Coefficient of Variation. ME: (Mean) Maximum Enhancement, Slope: Maximum observed enhancement slope between two time points, TTP: Time To Peak, VE: Volume of all enhancing pixels within the ROI. Tot = total number of pixels within the Region of Interest (ROI) classified to the specific Time Intensity Curve (TIC) shape type. Rel = number of pixels within the ROI classified to the specific TIC shape type relative to all enhancing pixels within the ROI.

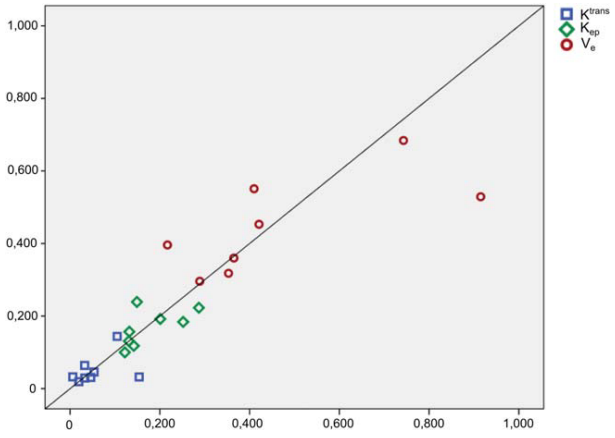

Figure 3.5 Measurement of K^{trans} (blue boxes), K_{ep} (green diamonds), and V_e (red circles) in Group 1 (2 x GE). Line: unity (y=x).

TIC-shape absolute and relative amounts

The absolute numbers of pixels showing TIC-shape types 2, 3, and 4 showed good to very good reproducibility, with ICC values ranging from 0.71 to 0.82. The absolute number of type 5 TIC-shape pixels, however, showed poor reproducibility, with an ICC value of 0.09. RMS-CoV ranged from 29.8% to 73.8%. The relative TIC-shape numbers showed poor to very good reproducibility, with ICC-values ranging from -0.30 to 0.92. RMS-CoV values ranged from 30.1% to 79.8% (Table 3.5).

Discussion

Our data show that within one MRI scanner, qualitative analysis is the most reproducible method, with TIC-shape analysis (total numbers) being almost as robust with comparable ICC-values but somewhat higher RMS-CoV values. Pharmacokinetic modeling shows the lowest within-scanner reproducibility.

Between scanners, the situation is more complex. Compared to the within-scanner reproducibility, the qualitative parameters showed much lower reproducibility, especially the parameter slope. This parameter, in the literature also referred to as IRE or EER, is often considered the most "important" and most responsive parameter when assessing disease activity with DCE-MRI in follow-up studies.[10,17,18,31] The total number of TIC-shapes per type showed ICCs similar to the qualitative analysis. In the TIC-shape analysis there are also two most "important" types of shapes, namely, the type showing "benign" gradual enhancement and no washout (our TIC-shape type 2) and the type showing "malignant" early enhancement and early washout (our type 4). These TIC-shape types 2 and 4 showed good ICC-values that are higher compared to the qualitative parameter slope. Therefore, we believe that TIC-shape analysis is more reliable compared to qualitative analysis when used in longitudinal studies with different scanners. More important, our results also show that between-scanner reproducibility of the TIC shape types 2 and 4 outperforms the intrascanner reproducibility of the PKM parameters. Despite the claim that PKM parameters should provide absolute values that can be directly compared between patients, in practice the process leading to the extraction of the PKM parameters, including the transformation from signal to concentration and the acquisition and fitting of the arterial input function (AIF), is very prone to errors. Although the use of a standard (population averaged) AIF has shown to improve reproducibility,[28] as the acquisition of a patient specific AIF increases the accuracy of the results, we chose to use the last method. It is possible that this has affected our reproducibility results.

The data on the reproducibility of DCE-MRI data in synovitis patients is limited to a few works that mainly assess the intra- and interobserver reliability of the qualitative parameters IRE/EER and ME. The intra- and interobserver agreement for these parameters has been proven reliable with ICCs for rate of enhancement (IRE/EER) of

0.91–1.00 and for ME of 0.93–1.00.[7,10,32–35] One publication showed a very good intraobserver agreement in TIC-shape analysis with an ICC of 1.0.[35] There are some publications about the reproducibility of DCE-MRI in arthritis patients within one scanner; Ostergaard et al.[16] observed an inter-MRI variation of 15% (whole synovium) and 27% (4 points of interest) in the qualitative parameter REE/IRE in six patients within 3 days. Hodgson et al.[14] measured the repeatability of PKM parameters in eight arthritis patients within 14 days within one scanner. A test–retest RMS-CoV of 27% was observed in the parameter K^{trans}, which is lower compared to our results. However, they also observed an RMS-CoV of 16% in the parameter v_e, which is only slightly lower compared to our obtained value and of 78% in the parameter plasma volume (v_p). Our most reproducible PKM parameter was the parameter K_{ep}.

It is assumed that qualitative parameters such as IRE/Slope and ME are scanner and scan parameter-dependent and that it is not possible to compare these values obtained by different scanners. Our results confirm these assumptions. However, despite the low ICC we observed for the parameter Slope, it has to be observed that the slope values across the scanners still retain a linear trend. The lower TIC-shape reproducibility we observed in the between-scanners study could be explained by the fact that the different T_1 weighting on different field strengths can still affect the shape classification results. The difference between shape 3, 4, and 5, for example, is determined by a threshold. This identifies a range of angles for the washout slope within which the last part of the TIC is classified as "flat" (type 3), decreasing (type 4), and increasing (type 5). We used the same thresholds for both scanners, but differences in T_1 weighting can affect this slope, resulting in lower reproducibility. The differences in the amount of pixels classified as type 2 and type 5 (steady slow enhancement and quick enhancement followed by slow enhancement) can be a result of the lower signal-to-noise ratio (SNR) on the 1.0T scanner. Sudden signal increases due to noise effects could have been mistaken for a quick enhancement. Overall, we observed higher ICC values and lower RMS-CoV values in the intrascanner reproducibility group compared to the between-scanner reproducibility group for both the qualitative parameters and the TIC-shape analysis. Therefore, if these parameters are used in follow-up scans (eg, to evaluate therapy response), the scans should by preference be performed on the same scanner. We were not able to assess the interscanner reproducibility of the PKM parameters, because at the time of acquisition we could not perform a reliable T_1 quantification on the open-bore 1.0T MRI-scanner and therefore we could not calculate the absolute contrast agent concentrations needed for the PKM. Based on the results obtained in the intrascanner reproducibility study, we believe that the PKM analysis would not outperform the TIC shape analysis on the interscanner study.

Our data show that the ICCs of the total number of the different TIC-shape types are higher compared to the relative number. We believe this is due to the statistical tests used. As the ICC compares the difference between the two measurements within one patient to the difference between all patients, the use of relative amounts results in the interpatient differences being somewhat reduced. However, the relative number of the

most "important" TIC-shape types (types 2 and 4, the "benign" and "malignant" types) show good and very good ICC values.

More and more, DCE-MRI is used to study arthritic diseases. Many studies apply this technique on single-slice acquisitions or predefined ROIs. TIC-shape analysis on a pixel-by-pixel basis is a relatively new post-processing technique that allows visualizing and quantifying the heterogeneity of the TIC behavior in the whole synovium. This makes it possible to identify the most "active" sites within the synovium, which may be indicative of the development of erosions, or can be used in the selection of synovial biopsy sites. It allows for the differentiation of healthy subjects and RA patients,[35] and might be able to assist in early differentiation of different disease entities, although in a previous study this was not proven.[9] It may also be used to assess disease activity in clinical or outpatient settings or monitor therapy response in clinical trials or in individual patients. Because the TIC shape analysis requires a much less cumbersome post-processing than that required for quantification with PK modeling, it can be more easily applied in routine patient care, and has therefore more potential to make an impact on it.

Some limitations of this study should be mentioned. The ICC tests used to test between the two sessions showed wide 95% confidence intervals, including a lower limit below the "poor" classification (<0.20), probably due to the small number of patients analyzed per group. Therefore, the outcomes should be carefully interpreted and preferably confirmed in larger patient groups. However, this is the largest group to be tested for reproducibility in arthritis patients so far. The scanner we used was relatively old, but has a relatively high field strength compared to other commonly used scanners (especially dedicated extremity scanners) in this field of research, and is still being used in clinical settings around the world. Unfortunately, the scanner was replaced during inclusion, which resulted in a premature stop of the inclusion of patients. For the TIC shape analysis as in,[2] thresholds are used in order to separate the different classes.

Thresholds used for the classifications were the same for all the scans conducted on the same scanner, while for group 2 the thresholds used were different between the two scans. The use of different thresholds might have influenced the different results.

In conclusion, we have shown that DCE-MRI TICshape analysis within one scanner is as robust and reliable compared to qualitative analysis and more reproducible compared to PKM analysis. However, the groups were small, so more research in larger groups should be performed to safely apply this technique in clinical settings, for example, as marker in the evaluation of therapeutic effect in longitudinal studies. We have also shown that DCE-MRI TIC-shape analysis between scanners is more robust compared to the use of the EER/Slope, especially when looking at the most clinically relevant TIC-shape types 2 and 4. More important, we have shown that the between-scanner reproducibility of the qualitative and TIC shape analysis outperforms the within-scanner reproducibility of the PKM analysis. These facts should be taken into consideration when planning to use different scanners and analytical techniques in follow-up studies or clinical practice.

References

1. Tofts PS, Brix G, Buckley DL, et al. Estimating kinetic parameters from dynamic contrast-enhanced T(1)-weighted MRI of a diffusable tracer: standardized quantities and symbols. J Magn Reson Imaging JMRI 1999;10:223–32.
2. Lavini C, de Jonge MC, van de Sande MGH, Tak PP, Nederveen AJ, Maas M. Pixel-by-pixel analysis of DCE MRI curve patterns and an illustration of its application to the imaging of the musculoskeletal system. Magn Reson Imaging 2007;25:604–12.
3. Cimmino MA, Parodi M, Innocenti S, et al. Dynamic magnetic resonance of the wrist in psoriatic arthritis reveals imaging patterns similar to those of rheumatoid arthritis. Arthritis Res Ther 2005;7:R725–31.
4. Kirkhus E, Bjørnerud A, Thoen J, Johnston V, Dale K, Smith H-J. Contrast-enhanced dynamic magnetic resonance imaging of finger joints in osteoarthritis and rheumatoid arthritis: an analysis based on pharmacokinetic modeling. Acta Radiol Stockh Swed 1987 2006;47:845–51.
5. Marzo-Ortega H, Tanner SF, Rhodes LA, et al. Magnetic resonance imaging in the assessment of metacarpophalangeal joint disease in early psoriatic and rheumatoid arthritis. Scand J Rheumatol 2009;38:79–83.
6. Marzo-Ortega H, Rhodes LA, Tan AL, et al. Evidence for a different anatomic basis for joint disease localization in polymyalgia rheumatica in comparison with rheumatoid arthritis. Arthritis Rheum 2007;56:3496–501.
7. Rhodes LA, Tan AL, Tanner SF, et al. Regional variation and differential response to therapy for knee synovitis adjacent to the cartilagepannus junction and suprapatellar pouch in inflammatory arthritis: implications for pathogenesis and treatment. Arthritis Rheum 2004;50:2428–32.
8. Schraml C, Schwenzer NF, Martirosian P, et al. Assessment of synovitis in erosive osteoarthritis of the hand using DCE-MRI and comparison with that in its major mimic, the psoriatic arthritis. Acad Radiol 2011;18:804–9.
9. Van de Sande MGH, van der Leij C, Lavini C, Wijbrandts CA, Maas M, Tak PP. Characteristics of synovial inflammation in early arthritis analysed by pixel-by-pixel time-intensity curve shape analysis. Rheumatology 2012;51:1240–5.
10. Axelsen MB, Poggenborg RP, Stoltenberg M, et al. Reliability and responsiveness of dynamic contrast-enhanced magnetic resonance imaging in rheumatoid arthritis. Scand J Rheumatol 2013;42:115–22.
11. Cimmino MA, Barbieri F, Boesen M, et al. Dynamic contrastenhanced magnetic resonance imaging of articular and extraarticular synovial structures of the hands in patients with psoriatic arthritis. J Rheumatol Suppl 2012;89:44–8.
12. Fritz J, Galeczko EK, Schwenzer N, et al. Longitudinal changes in rheumatoid arthritis after rituximab administration assessed by quantitative and dynamic contrast-enhanced 3-T MR imaging: preliminary findings. Eur Radiol 2009;19:2217–24.
13. Hodgson RJ, Barnes T, Connolly S, Eyes B, Campbell RSD, Moots R. Changes underlying the dynamic contrast-enhanced MRI response to treatment in rheumatoid arthritis. Skeletal Radiol 2008;37:201–7.
14. Hodgson RJ, Connolly S, Barnes T, Eyes B, Campbell RSD, Moots R. Pharmacokinetic modeling of dynamic contrast-enhanced MRI of the hand and wrist in rheumatoid arthritis and the response to anti-tumor necrosis factor-alpha therapy. Magn Reson Med 2007;58:482–9.
15. Kalden-Nemeth D, Grebmeier J, Antoni C, Manger B, Wolf F, Kalden JR. NMR monitoring of rheumatoid arthritis patients receiving anti-TNF-alpha monoclonal antibody therapy. Rheumatol Int 1997;16: 249-55.
16. Ostergaard M, Stoltenberg M, Henriksen O, Lorenzen I. Quantitative assessment of synovial inflammation by dynamic gadoliniumenhanced magnetic resonance imaging. A study of the effect of intraarticular methylprednisolone on the rate of early synovial enhancement. Br J Rheumatol 1996;35:50–9.
17. Reece RJ, Kraan MC, Radjenovic A, et al. Comparative assessment of leflunomide and methotrexate for the treatment of rheumatoid arthritis, by dynamic enhanced magnetic resonance imaging. Arthritis Rheum 2002;46:366–72.

18. Tam L-S, Griffith JF, Yu AB, Li TK, Li EK. Rapid improvement in rheumatoid arthritis patients on combination of methotrexate and infliximab: clinical and magnetic resonance imaging evaluation. Clin Rheumatol 2007;26:941–6.
19. Veale DJ, Reece RJ, Parsons W, et al. Intra-articular primatised anti-CD4: efficacy in resistant rheumatoid knees. A study of combined arthroscopy, magnetic resonance imaging, and histology. Ann Rheum Dis 1999;58:342–9.
20. De Hair MJH, Harty LC, Gerlag DM, Pitzalis C, Veale DJ, Tak PP. Synovial tissue analysis for the discovery of diagnostic and prognostic biomarkers in patients with early arthritis. J Rheumatol 2011;38:2068–72.
21. Arnett FC, Edworthy SM, Bloch DA, et al. The American Rheumatism Association 1987 revised criteria for the classification of rheumatoid arthritis. Arthritis Rheum 1988;31:315–24.
22. Altman R, Asch E, Bloch D, et al. Development of criteria for the classification and reporting of osteoarthritis. Classification of osteoarthritis of the knee. Diagnostic and Therapeutic Criteria Committee of the American Rheumatism Association. Arthritis Rheum 1986;29:1039–49.
23. Dougados M, van der Linden S, Juhlin R, et al. The European Spondylarthropathy Study Group preliminary criteria for the classification of spondylarthropathy. Arthritis Rheum 1991;34:1218–27.
24. Petty RE, Southwood TR, Manners P, et al. International League of Associations for Rheumatology classification of juvenile idiopathic arthritis: second revision, Edmonton, 2001. J Rheumatol 2004;31:390–2.
25. McCarty DJ, O'Duffy JD, Pearson L, Hunter JB. Remitting seronegative symmetrical synovitis with pitting edema. RS3PE syndrome. JAMA 1985;254:2763–7.
26. Lavini C, Maas M. DCE-MRI analysis package comprising pixel-bypixel classification of Time Intensity Curves shapes, permeability maps and Gd concentration calculation. Magn Reson Mater Phys Biol Med 2008;21:486.
27. Schabel MC, Parker DL. Uncertainty and bias in contrast concentration measurements using spoiled gradient echo pulse sequences. Phys Med Biol 2008;53:2345–73.
28. Parker GJM, Roberts C, Macdonald A, et al. Experimentally-derived functional form for a population-averaged high-temporal-resolution arterial input function for dynamic contrast-enhanced MRI. Magn Reson Med 2006;56:993–1000.
29. Orton MR, d' Arcy JA, Walker-Samuel S, et al. Computationally efficient vascular input function models for quantitative kinetic modelling using DCE-MRI. Phys Med Biol 2008;53:1225–39.
30. Roberts C, Issa B, Stone A, Jackson A, Waterton JC, Parker GJM. Comparative study into the robustness of compartmental modeling and model-free analysis in DCE-MRI studies. J Magn Reson Imaging JMRI 2006;23:554–63.
31. Ostergaard M, Stoltenberg M, Gideon P, Sørensen K, Henriksen O, Lorenzen I. Changes in synovial membrane and joint effusion volumes after intraarticular methylprednisolone. Quantitative assessment of inflammatory and destructive changes in arthritis by MRI. J Rheumatol 1996;23:1151–61.
32. Axelsen MB, Stoltenberg M, Poggenborg RP, et al. Dynamic gadolinium-enhanced magnetic resonance imaging allows accurate assessment of the synovial inflammatory activity in rheumatoid arthritis knee joints: a comparison with synovial histology. Scand J Rheumatol 2012;41:89–94.
33. Huang J, Stewart N, Crabbe J, et al. A 1-year follow-up study of dynamic magnetic resonance imaging in early rheumatoid arthritis reveals synovitis to be increased in shared epitope-positive patients and predictive of erosions at 1 year. Rheumatology 2000;39:407–16.
34. Palosaari K, Vuotila J, Takalo R, et al. Contrast-enhanced dynamic and static MRI correlates with quantitative 99Tcm-labelled nanocolloid scintigraphy. Study of early rheumatoid arthritis patients. Rheumatology 2004;43:1364–73.
35. Van der Leij C, van de Sande MGH, Lavini C, Tak PP, Maas M. Rheumatoid synovial inflammation: pixel-by-pixel dynamic contrastenhanced MR imaging time-intensity curve shape analysis—a feasibility study. Radiology 2009;253:234–40.